

Twisted skyrmion at domain boundaries and the method of image

Huanhuan Yang, C. Wang,* Xiaofan Wang, X.S. Wang, Yunshan Cao, and Peng Yan†

School of Microelectronics and Solid-state Electronics and State Key Laboratory of Electronic Thin Film and Integrated Devices,
University of Electronic Science and Technology of China, Chengdu 610054, China

(Dated: March 8, 2018)

We predict a novel twisted skyrmion structure at the boundary of two antiferromagnetically coupled magnetic domains with antiparallel magnetization directions. Through this intermediate state, skyrmions with opposite polarities can be freely switched between each other by spin-polarized electric currents. Based on these findings, we propose the concept of double-track skyrmion racetrack memory and logic gates where the binary data are represented by skyrmions with different polarities. The dynamics of skyrmion polarity reversal is theoretically studied. Using the method of image, we derive the analytical formula of the repulsive potential when a normal skyrmion approaches the domain boundary. A harmonic attractive potential well is obtained for the twisted skyrmion across the boundary. Micromagnetic simulations compare well with theoretical predictions. The method of image skyrmion proposed in this work can be used to deal with a large class of skyrmion-boundary interaction problems.

Introduction.—Magnetic skyrmions are stable swirling non-coplanar topological defects in the magnetization texture. Since the theoretical prediction more than two decades ago [1, 2] and the recent experimental observation [3], intensive investigation on magnetic skyrmions gives birth to an emerging subfield of condensed matter physics, the skyrmionics [4–7]. Due to their small size, excellent stability and low driving current, skyrmions are promising information carriers in future ultra-dense (and -fast) spintronic applications, of which the most attractive proposals are skyrmion racetrack memories (SRMs) and skyrmion logic gates (SLGs), while data representation is still a key obstacle. Unlike their domain-wall counterpart [8, 9] where the binary data bits “1” and “0” are encoded by magnetic domains of opposite spin directions integrated with the magnetoresistive (MR) sensor, it is impossible to reverse the core polarity of a single skyrmion on the track, unless all spins of the magnetic domain are switched [10, 11]. The topologically protected stability of magnetic skyrmions is thus double-edged. A compromised approach is to represent “1” and “0” by the presence and absence of a skyrmion (or the other way around), respectively. This method, however, requires an exactly synchronized motion of all skyrmions. If there is a pinning or any relative motion between the skyrmions, errors happen inevitably, and one cannot identify the errors from normal data. Although there are proposals of two-lane SRM in the literature claimed to overcome the problem [12, 13], a reliable data representation is still not achieved since those proposals rely on the presence and absence of skyrmions, instead of skyrmions carrying opposite polarities.

Tantalizing physics often emerges at boundaries, such as the recently discovered quantum spin Hall insulator states [14] and chiral majorana fermion modes [15], among others. As to magnetic skyrmions, the edge effect in most cases is viewed as harmful because the intrinsic skyrmion Hall effect tends to result in skyrmion accumulations there. Even worse, skyrmions can be annihilated by the edge. How skyrmions interact with the boundary is not solved in a satisfactory manner in the community. In this Letter, we predict a novel stable

twisted skyrmion state at the boundary of two antiferromagnetically (AFM) coupled magnetic domains aligned in an antiparallel way (shown in Fig. 1). Through this intermediate state, skyrmions in the two domains can be freely switched between each other by, for example, applying an electric current. This enables us to design a double-track SRM, as well as SLGs, in which skyrmions with opposite polarities are utilized to encode “1” and “0”. Our proposal removes the mentioned barrier for achieving the SRM and SLG. Furthermore, using the method of image, we derive the analytical formula of the potential energy when a normal skyrmion approaches the domain boundary. Our analytical results show that the potential is repulsive and inversely proportional to the square of the distance between the skyrmion and the boundary in the large distance limit, while it becomes linear when the skyrmion is very close to the boundary. After the skyrmion steps into the domain boundary, a twisted skyrmion forms and is confined by a harmonic attractive potential well. Micromagnetic simulations compare very well with theoretical predictions. The method of image skyrmion we developed can be used to solve a large class of skyrmion-boundary interaction problems.

Model.—We start from the following classical spin Hamiltonian in two spatial dimensions ($x - y$ plane),

$$\mathcal{H} = - \sum_{\langle ij \rangle \notin B} J_{\text{FM}}(\mathbf{m}_i \cdot \mathbf{m}_j) + \sum_{\langle ij \rangle \in B} J_{\text{AFM}}(\mathbf{m}_i \cdot \mathbf{m}_j) - \sum_{\langle ij \rangle} \mathbf{D}_{ij} \cdot (\mathbf{m}_i \times \mathbf{m}_j) - \sum_i K(\mathbf{m}_i \cdot \hat{z})^2 + \mathcal{H}_{\text{DDI}}. \quad (1)$$

Here \mathbf{m}_i is the unit vector of spin at the site $i = (i_x a, i_y a)$ ($i_{x(y)}$ is an integer and a is the lattice constant) with saturation magnetization M . $\langle ij \rangle \notin B$ ($\langle ij \rangle \in B$) sums over all nearest-neighbour sites away from (at) the boundary. $J_{\text{FM}} > 0$ is the ferromagnetic exchange constant in magnetic domains, and $J_{\text{AFM}} > 0$ is the AFM exchange coupling at the boundary of two domains with antiparallel-aligned magnetizations [see Fig. 1(b)]. The third term in the right hand of Eq. (1) represents the interfacial Dzyaloshinskii-Moriya interaction (DMI) with a homogeneous DMI vector $\mathbf{D}_{ij} = D \hat{r}_{ij} \times \hat{z}$, where \hat{r}_{ij} is the unit vector connecting sites i and j . Parameter $K > 0$ is

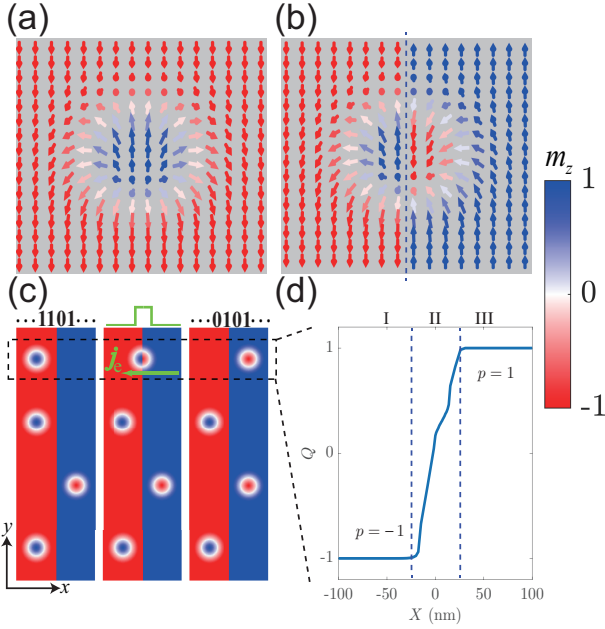


FIG. 1: (a)(b) Illustration of a normal skyrmion in a single magnetic domain (a) and a twisted skyrmion at the boundary (dashed line) of two antiparallel magnetic domains (b). (c) Schematics (top view) of four bits consisting of four skyrmions in a double-track SRM. A local electric current (green arrow) is injected along x -axis (electrons move from left to right) to drive the first skyrmion across the boundary, and to flip its core polarity at the same time, so that the binary data “1101” is rewritten to be “0101”. (d) Position dependence of the skyrmion charge Q . Its polarity p changes the sign after the skyrmion passes through the boundary.

the easy-axis uniaxial anisotropy constant along z -direction. \mathcal{H}_{DDI} is the dipole-dipole interaction energy. A Néel-type skyrmion is favored in this model Hamiltonian.

Creation of the twisted skyrmion.—By applying electric current, we can push a normal Néel skyrmion [shown Fig. 1(a)] into the domain boundary where the skyrmion structure is strongly twisted due to the large interfacial AFM interaction [shown Fig. 1(b)]. To test this idea, we have performed micromagnetic simulations with the MuMax3 package [16], using materials parameters of cobalt/platinum (CoPt) [17] with the DMI $D = 1.4$ meV, the ferromagnetic exchange constant $J_{\text{FM}} = 94$ meV, the uniaxial anisotropy $K = 0.07$ meV, the saturation magnetization $M = 5.8 \times 10^5$ A m $^{-1}$, the Gilbert damping constant $\alpha = 0.3$, and the boundary AFM energy $J_{\text{AFM}} = 0.05 - 3 J_{\text{FM}}$. We consider a sample of size $600 \times 2000 \times 1$ nm 3 with the lattice constant $a = 1$ nm.

One example of twisted skyrmion creation and its dynamics is depicted in Fig. 1(c). The boundary separating the two domains is at $x = 0$. We choose an interfacial AFM constant $J_{\text{AFM}} = J_{\text{FM}}$, and consider a single Néel skyrmion with polarity $p = -1$ initially in the left magnetic domain (the skyrmion polarity is defined as follows: $p = \mp 1$ corresponds to the core spin pointing up and down, respectively). Then, we inject a very large in-plane electric current $\mathbf{j}_e = -j_e \hat{x}$ with $j_e = 10^{13}$

A m $^{-2}$, to drive the skyrmion to propagate toward the boundary. The skyrmion crosses the boundary and transforms into a twisted skyrmion, as shown in the middle panel of Fig. 1 (c). We find that the twisted skyrmion stops at the boundary if the current is turned off at this moment. This result indicates that the twisted skyrmion is also a stable magnetic soliton. As the electric current is still on, the twisted skyrmion will keep moving and leave the boundary. Finally it recovers the normal state in the opposite domain, however, with a reversed polarity $p = 1$, as shown in the right panel of Fig. 1(c). Spin transfer torques under a different configuration, i.e., current perpendicular to plane, as well as the spin-orbit/spin Hall torques originating from the relativistic spin orbital coupling can also be adopted to drive the skyrmion propagation and its polarity switching [18]. Consequently, we can use $p = \mp 1$ to encode the binary bits “1” and “0” in a double-track SRM, as shown in Fig. 1 (c). This encoding approach is quite robust against external frustrations. For instance, if one skyrmion is pinned, the double-track SRM with integrated MR sensors is able to distinguish the error from normal data [18]. Skyrmion logic based on the novel data representation concept is also proposed and validated [18].

Figure 1(d) shows the topological charge $Q = \int q d\mathbf{r}$ as a function of the position of the skyrmion (twisted skyrmion) center plotted in Fig. 1(c). Here $q(\mathbf{r}) = \mathbf{m} \cdot (\partial_x \mathbf{m} \times \partial_y \mathbf{m}) / (4\pi)$ is the skyrmion charge density expressed in the continuum limit. The skyrmion (twisted skyrmion) center is defined as $\mathbf{X} = (X, Y) \equiv Q^{-1} \int q \mathbf{r} d\mathbf{r}$. We find that there exist two plateaus, $Q = -1$ and 1 , corresponding to the state that the skyrmion is in the left and right domains with $p = -1$ and 1 , respectively. For the twisted skyrmion state, Q changes continuously with X .

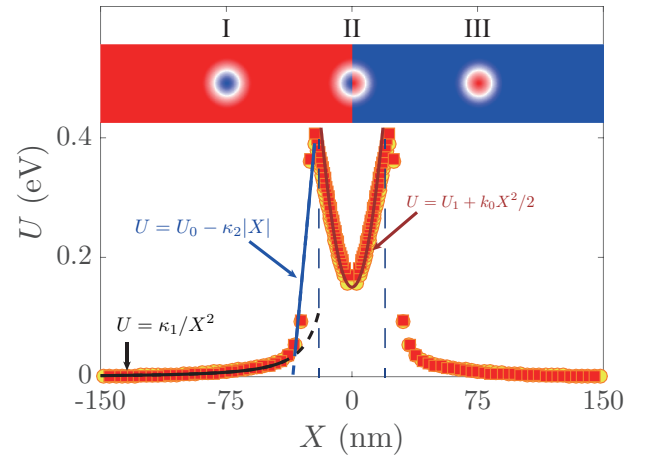


FIG. 2: Potential energy U v.s. skyrmion/twisted skyrmion center position X for $J_{\text{AFM}}/J_{\text{FM}} = 1$ (yellow circles) and 3 (red squares). The solid black curve is Eq. (4a) with $R = 12$ nm. The solid blue line is Eq. (4b) with a smaller $R = 5$ nm due to the size shrinking (not shown) of skyrmion when it is very close to the boundary. The solid brown curve is Eq. (5) with $R = 20$ nm, $R' = 4.5$ nm, and $U_1 = 0.15$ eV obtained from the micromagnetic simulations. Inset: three representative skyrmion structures in different regions.

To have a better understanding of the physics associated with the skyrmion polarity reversal, we numerically compute the potential energy $U(\mathbf{X})$ of the skyrmion, defined as the difference between the energy of a skyrmion/twisted skyrmion at \mathbf{X} and the energy U_0 of a skyrmion at the center of the left domain ($X = -150$ nm). Two representative numerical results of $U(X)$ for $J_{\text{AFM}}/J_{\text{FM}} = 1$ and 3 are shown by circles and squares, respectively, in Fig. 2. We find that the behavior of the potential can be divided into three regimes I, II, and III [shown in the inset of Fig. 2]. Regime I corresponds to the case that the skyrmion is in the left domain, in which U increases when $|X|$ decreases. The boundary exerts a repulsive force which balances the Magnus force, and thus suppresses the skyrmion Hall effect. Therefore, if we put more skyrmions in the double track, all those skyrmions will move synchronously parallel with the boundary [18]. The potential U keeps increasing until it goes very close to the boundary, i.e., $-20 \text{ nm} < X \leq 0$ nm. Driven by the large electric current, the skyrmion is able to overcome the energy barrier and to step into the regime II ($|X| \leq 20$ nm), forming a twisted skyrmion structure, in which an attractive potential well with its energy minimum at $X = 0$ is clearly observed. Because the applied current is large enough, the twisted skyrmion is pushed out of the potential well, and transforms back to a normal skyrmion state with opposite polarity in regime III. In the following, we quantitatively explain the potential curves obtained in all regimes.

Method of image skyrmions.—We first focus on regime I where the normal skyrmion is approaching the domain boundary. The situation in regime III is identical because of symmetry. Up to now, it is still an open question on the form of the potential/force from the boundary in the skyrmionic community. A number of numerical studies have been reported in the literature [19–23] employing empirical formulae, such as the quadratic potential [19] and the exponential one [20–23], without analytical justifications. It is thus of great importance and high interest to know the exact form of the potential U between the skyrmion and the boundary. Here, we derive the analytical expression of U , to the best of our knowledge for the first time. Our analytical results show that neither the harmonic nor the exponential potential is a good description. To quantitatively formulate the problem, we write the magnetization profile of a skyrmion as $\mathbf{m}(\mathbf{r}) = (\cos \Phi(\phi) \sin \Theta(r), \sin \Phi(\phi) \sin \Theta(r), \cos \Theta(r))$, where Φ depends only on angular coordinate ϕ and Θ relies only on radial coordinate r , measured from its center \mathbf{X} .

The general solution for the in-plane angle of a static symmetric skyrmion reads $\Phi(\phi) = m\phi + \eta$, where m is the vorticity and η is the phase angle [24]. Remarkably, we notice that $\Phi(\phi)$ satisfies the two-dimensional Laplace equation

$$\nabla^2 \Phi = 0. \quad (2)$$

This fact motivates us to consider the method of image to solve the skyrmion-boundary interaction problem, as long as the skyrmion has a good point-like particle nature. This is justified if the skyrmion does not significantly overlap with its

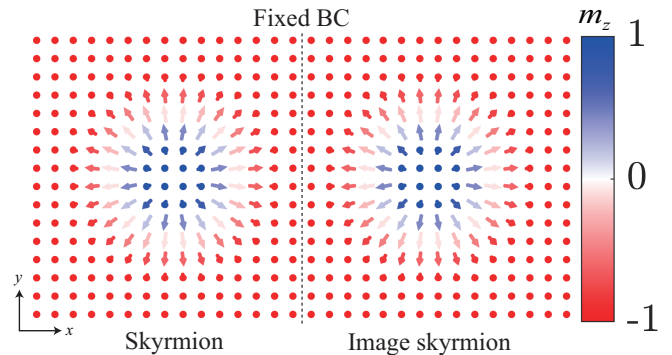


FIG. 3: Schematic of the method of image in the skyrmion-boundary interaction problem. The original skyrmion is in left domain with the center coordinate (X, Y) and its image locates in the right domain with the center coordinate $(-X, Y)$. Dash line represents the boundary.

image. Of course, the properties of the image skyrmion exclusively depend on the boundary condition. In our model Hamiltonian, we have introduced an interfacial AFM exchange coupling, so the edge spins in the left domain are strongly pinned by the right magnetic domain. This corresponds to the fixed boundary condition (BC) or the Dirichlet BC:

$$\mathbf{m}(\mathbf{r}) \cdot \mathbf{n}|_{\mathbf{r} \in \text{B}} = 0, \quad (3)$$

where \mathbf{n} is the normal direction of the boundary. We infer that the image skyrmion locates at $(-X, Y)$, assuming the original skyrmion at (X, Y) , with magnetization configuration exactly being the mirror image of the original skyrmion with respect to the boundary, to satisfy the Dirichlet BC, as shown in Fig. 3 (see the proof in Supplemental Materials [18]). Then the potential due to the boundary is equivalent to the interacting energy of the skyrmion|image-skyrmion pair. Its analytical form is obtained [18], with very simple forms in the following two limits

$$U(X) = \begin{cases} \kappa_1/X^2 & \text{for } |X| \gg R, \\ U_0 - \kappa_2|X| & \text{for } |X| \gtrsim R. \end{cases} \quad (4a)$$

$$(4b)$$

Here $\kappa_1 = 3\pi J_{\text{FM}} R^2/8$ with R the radius of the skyrmion, and κ_2 and U_0 are functions of J_{FM} and R . The agreement of our analytical formula (4a) and (4b) with micromagnetic simulations appears to be very well (shown in Fig. 2). We would like to remark that Eq. (2) is generally true for symmetric skyrmion structures. Therefore, the method of image skyrmions can be utilized to solve a large class of skyrmion-boundary interaction problems, e.g. skyrmions in confined geometry with curved boundaries. The Dirichlet BC can also be replaced by other types of BCs, such as the Neumann BC (free BC) and the Robin BC, depending on the physical situations. Bloch skyrmion and antiskyrmion can be similarly treated as well. A thorough investigation on the application of the method of image skyrmions will be published elsewhere [25].

Harmonic potential at the boundary.—In regime II, the method of image skyrmion is not valid any more because the skyrmion is not a good point-like particle and has a significant overlap with its image. However, we find that the derivation of the potential is unexpectedly simple for the twisted skyrmion at boundaries. It turns out to be a harmonic potential well [18],

$$U(X) = U_1 + \frac{k_0}{2}X^2, \text{ for } |X| < R, \quad (5)$$

where $U_1 = U(X = 0)$ is the energy minimum of the twisted skyrmion, and $k_0 = 2J_{\text{FM}}R'/(aR^2)$ is an effective spring constant with R (R') the length of the semi-major (semi-minor) axis of the deformed twisted skyrmion with an elliptical shape. We find that the numerically calculated $U(X)$ ($|X| < R$) can be well described by Eq. (5) (see Fig. 2).

Phase diagram.—In previous simulations, we applied an electric current density as high as 10^{13} A m $^{-2}$, and identified three different skyrmion states: $p = -1$ skyrmion, twisted skyrmion, and $p = +1$ skyrmion. It is not clear what will happen if we significantly lower the current density and/or the interfacial AFM coupling. In order to obtain a complete picture, we now calculate the phase diagram by tuning the mentioned two parameters j_e and J_{AFM} . Numerical results are shown in Fig. 4, in which we find four phases, labeled as “S” (skyrmion successfully passes through the boundary and flips its polarity), “T” (skyrmion is trapped at the boundary), “A” (skyrmion annihilates at the boundary), and “R” (skyrmion is rejected by the boundary), respectively. The phase diagram is thus called STAR (see Supplemental Materials [18] for movies visualizing the skyrmion motion in different phases). In the limit of a strong interfacial AFM coupling, the STAR phase diagram shows that both the skyrmion and the twisted skyrmion are stable. Substituting Eqs. (4b) and (5) into the Thiele’s equation [26, 27], we are able to obtain two critical currents [18]

$$j_{c,1} = \frac{\gamma|e|(1 + \beta^2)\alpha\mathcal{D}\kappa_2}{(16\pi^2 + \alpha\beta\mathcal{D}^2)a\mu_B} \quad \text{and} \quad j_{c,2} = \frac{k_0R}{\kappa_2}j_{c,1}, \quad (6)$$

for the phase transition R \rightarrow T and T \rightarrow S, respectively.

In the above equations, $\mathcal{D} = \int(\partial_x\mathbf{m})^2d\mathbf{r}$, β is the nonadiabatic spin torque parameter (it is set to be 0.3 in micromagnetic simulations), γ is the (positive) gyromagnetic ratio, e is the electron charge, and μ_B is the Bohr magneton. Analytical formula agrees excellently with numerical results. For a small J_{AFM} , the skyrmion may annihilate at the boundary (phase “A”) when a moderate current is applied, indicating a finite skyrmion life-time at the boundary [28]. However, a large enough current can still drive the skyrmion to cross the boundary (phase “S”) before its annihilation, as long as the tunneling time is much shorter than its life-time. The existence of the phase transition A \rightarrow S indicates that the realization of double-track SRM actually does not rely on a very large interfacial AFM coupling.

Material considerations.—The AFM coupled ferromagnetic domains is essential to our proposal, which fortunately has been found to exist in the martensite phase of the Heusler-type

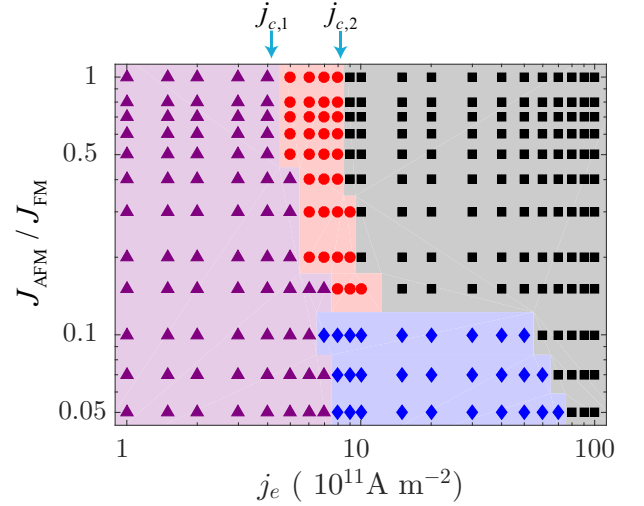


FIG. 4: STAR phase diagram plotted in the $J_{\text{AFM}}-j_e$ plane, with black squares for “S”, red circles for “T”, blue rhombus for “A”, and purple triangles for “R”. Arrows label the two critical currents $j_{c,1}$ and $j_{c,2}$ analytically obtained in the large J_{AFM} limit.

magnetic shape memory alloy [29]. Interestingly, a recent experiment reported the observations of magnetic antiskyrmions in the tetragonal Heusler materials above room temperature [30]. The Heusler materials are therefore promising systems for implementing the proposed SRM and SLGs. In addition, the twisted skyrmions can also be observed in the Fe-Cr-Fe multilayer and the Gd-Fe core-shell structure [31, 32], the cross sections of which can support the required AFM couplings between two ferromagnetic domains. The interfacial DMI can be generated by engineering the surface properties of these materials and structures [33].

To conclude, we reported a novel twisted skyrmion structure at the boundary separating two antiparallely aligned magnetic domains with antiferromagnetic interface coupling. We showed that skyrmions with opposite core polarities can be switched through the twisted skyrmion state. The major obstacle of data representation to achieve the SRM and SLGs is thus removed. We developed a method of image skyrmions to handle the boundary effect on the skyrmion, and obtained an analytical formula of boundary potential for the first time. The STAR phase diagram obtained should be useful to guide the design of the double-track SRM and SLGs. All analytical formulae are well supported by micromagnetic simulations. Materials and structures to realize our proposals are also discussed. We believe that our findings will shed new lights on both the fundamental sciences and the appealing applications of skyrmions.

We thank X.R. Wang for helpful discussion. This work is supported by the National Natural Science Foundation of China (Grants No. 11604041 and 11704060), the National Key Research Development Program under Contract No. 2016YFA0300801, and the National Thousand-Young-Talent Program of China. C.W. acknowledges the finan-

cial support from the China Postdoctoral Science Foundation (Grants No. 2017M610595 and 2017T100684) and the National Nature Science Foundation of China under Grant No. 11704061. X.S.W. is supported by the China Postdoctoral Science Foundation under Grant No. 2017M612932.

H.H.Y. and C.W. contributed equally to this work.

* corresponding author: cwangad@connect.ust.hk

† corresponding author: yan@uestc.edu.cn

- [1] N. Bogdanov and D.A. Yablonskii, Thermodynamically stable “vortices” in magnetically ordered crystals: the mixed state of magnets, *Sov. Phys. JETP* **68**, 101 (1989).
- [2] N. Bogdanov and A. Hubert, Thermodynamically stable magnetic vortex states in magnetic crystals, *J. Magn. Magn. Mater.* **138**, 255 (1994).
- [3] S. Mülbauer, B. Binz, F. Jonietz, C. Pfleiderer¹, A. Rosch, A. Neubauer, R. Georgii, P. Böni, Skyrmion lattice in a chiral magnet, *Science* **323**, 915 (2009).
- [4] R. Wiesendanger, Nanoscale magnetic skyrmions in metallic films and multilayers: a new twist for spintronics, *Nat. Rev. Mater.* **1**, 16044 (2016).
- [5] A. Fert, N. Reyren and V. Cros, Magnetic skyrmions: advances in physics and potential applications, *Nat. Rev. Mater.* **2**, 17031 (2017).
- [6] W. Jiang, G. Chen, K. Liu, J. Zang, S.G.E. te Velthuis, and Axel Hoffmann, Skyrmions in magnetic multilayers, *Phys. Rep.* **704**, 1 (2017).
- [7] S.K. Kim, K.-J. Lee, and Y. Tserkovnyak, Self-focusing skyrmion racetracks in ferrimagnets, *Phys. Rev. B* **95**, 140404(R) (2017).
- [8] S.S.P. Parkin, M. Hayashi, and L. Thomas, Magnetic domain-wall racetrack memory, *Science* **320**, 190 (2008).
- [9] D.A. Allwood, G. Xiong, C.C. Faulkner, D. Atkinson, D. Petit, and R.P. Cowburn, Magnetic Domain-Wall Logic, *Science* **309**, 1688 (2005).
- [10] C. Heo, N.S. Kiselev, A.K. Nandy, S. Blügel, and Theo Rasing, Switching of chiral magnetic skyrmions by picosecond magnetic field pulses via transient topological states, *Sci. Rep.* **6**, 27146 (2016).
- [11] F. Zheng, H. Li, S. Wang, D. Song, C. Jin, W. Wei, A. Kovács, J. Zang, M. Tian, Y. Zhang, H. Du, and R.E. Dunin-Borkowski, Direct Imaging of a Zero-Field Target Skyrmion and Its Polarity Switch in a Chiral Magnetic Nanodisk, *Phys. Rev. Lett.* **119**, 197205 (2017).
- [12] Wang Kang, Yangqi Huang, Xichao Zhang, Yan Zhou, and Weisheng Zhao, *Proc. IEEE*, **104**, 2040 (2016).
- [13] Jan Müller, Magnetic skyrmions on a two-lane racetrack, *New J. Phys.* **19**, 025002 (2017).
- [14] M. König, S. Wiedmann, C. Brüne, A. Roth, H. Buhmann, L.W. Molenkamp, X.-L. Qi, and S.-C. Zhang, Quantum Spin Hall Insulator State in HgTe Quantum Wells, *Science* **318**, 766 (2007).
- [15] Qin Lin He, Lei Pan, Alexander L. Stern, Edward C. Burks, Xiaoyu Che, Gen Yin, Jing Wang, Biao Lian, Quan Zhou, Eun Sang Choi et al., Chiral Majorana fermion modes in a quantum anomalous Hall insulator superconductor structure, *Science* **357**, 294 (2017).
- [16] A. Vansteenkiste, J. Leliaert, M. Dvornik, M. Helsen, F. Garcia-Sanchez, and B. Van Waeyenberge, The design and verification of MuMax3, *AIP Adv.* **4** 107133 (2014).
- [17] J. Sampaio, V. Cros, S. Rohart, A. Thiaville, and A. Fert, Nucleation, stability and current-induced motion of isolated magnetic skyrmions in nanostructures, *Nat. Nano.* **8**, 839 (2013).
- [18] See Supplemental Material at <http://link.aps.org/supplemental>.
- [19] J. Iwasaki, W. Koshibae, and N. Nagaosa, Colossal Spin Transfer Torque Effect on Skyrmion along the Edge, *Nano Lett.* **14**, 4432 (2014).
- [20] X. Zhang, G.P. Zhao, H. Fangohr, J.P. Liu, W.X. Xia, J. Xia, and F. J. Morvan, Skyrmion-skyrmion and skyrmion-edge repulsions in skyrmion-based racetrack memory, *Sci. Rep.* **5**, 7643 (2015).
- [21] X. Zhang, J. Müller, J. Xia, M. Garst, X. Liu, and Y. Zhou, Motion of skyrmions in nanowires driven by magnonic momentum-transfer forces, *New J. Phys.* **19**, 065001 (2017).
- [22] M.W. Yoo, V Cros, and J.V. Kim, Current-driven skyrmion expulsion from magnetic nanostrips, *Phys. Rev. B* **95**, 184423 (2017).
- [23] C. Navau, N. Del-Valle, and A. Sanchez, Analytical trajectories of skyrmions in confined geometries: Skyrmionic racetracks and nano-oscillators, *Phys. Rev. B* **94**, 184104 (2016).
- [24] N. Nagaosa and Y. Tokura, Topological properties and dynamics of magnetic skyrmions, *Nat. Nano.* **8**, 899 (2013).
- [25] Huanhuan Yang et al., in preparation.
- [26] A. A. Thiele, Steady-State Motion of Magnetic Domains, *Phys. Rev. Lett.* **30**, 230 (1973).
- [27] A. Thiaville, Y. Nakatani, J. Miltat, and Y. Suzuki, Micromagnetic understanding of current-driven domain wall motion in patterned nanowires, *Europhys. Lett.* **69**, 990 (2005).
- [28] P.F. Bessarab, G.P. Müller, I.S. Lobanov, F.N. Rybakov, N.S. Kiselev, H. Jónsson, V.M. Uzdin, S. Blügel, L. Bergqvist, and A. Delin, Lifetime of racetrack skyrmions, arXiv:1706.07173.
- [29] V. O. Golub, V. A. Lvov, I. Aseguinolaza, O. Salyuk, D. Popadiuk, Y. Kharlan, G. N. Kakazei, J. P. Araujo, J. M. Barandiaran, and V. A. Chernenko, Antiferromagnetic coupling between martensitic twin variants observed by magnetic resonance in Ni-Mn-Sn-Co films, *Phys. Rev. B* **95**, 024422 (2017).
- [30] Ajaya K. Nayak, Vivek Kumar, Tianping Ma, Peter Werner, Eckhard Pippel, Roshnee Sahoo, Françoise Damay, Ulrich K. Röbber, Claudia Felser, and Stuart S. P. Parkin, Magnetic anti-skyrmions above room temperature in tetragonal Heusler materials, *Nature* **548**, 561 (2017).
- [31] G. Binash, P. Grünberg, F. Saurenbach, and W. Zinn, Enhanced magnetoresistance in layered magnetic structures with antiferromagnetic interlayer exchange, *Phys. Rev. B* **39**, 4828 (1989).
- [32] N.R. Anderson and R.E. Camley, Temperature-dependent magnetization in bimagnetic nanoparticles with antiferromagnetic interfacial exchange, *Phys. Rev. B* **94**, 134432 (2016).
- [33] Hongxin Yang, André Thiaville, Stanislas Rohart, Albert Fert, and Mairbek Chshiev, Anatomy of Dzyaloshinskii-Moriya Interaction at Co/Pt Interfaces, *Phys. Rev. Lett.* **115**, 267210 (2015).